Sensorless Control of Synchronous Machine with an Inverter Integrated Rotor

Sehwa Choe, Eunsoo Jung, and Seung-Ki Sul
Seoul national university Power Electronics Center (SPEC)
Seoul National University
Seoul, Korea
sehwa@eepel.snu.ac.kr, eunsoo@eepel.snu.ac.kr, sulsk@plaza.snu.ac.kr

***Abstract*—This paper proposes a new sensorless method for a Synchronous Machine with an Inverter Integrated Rotor (SMIIR). The SMIIR is a newly developed machine based on the wound rotor synchronous machine (WRSM) but has no brushes and slip-rings. And conventional high-frequency signal injection sensorless methods are based on physical magnetic saliency. Therefore, conventional methods cannot be applied to the SMIIR which has no sufficient magnetic saliency. The proposed sensorless method suggests virtual resistance saliency created by the rotor-side inverter, whose axes can be placed arbitrarily. Based on this virtual saliency the rotor position information is included and excluded in the relationship between the high-frequency stator voltage and stator current. Because the SMIIR already injects high-frequency voltage for the power transfer, there is no need to inject additional voltage for the proposed high-frequency sensorless method. And initial +d axis detection algorithm using the rotor-side inverter without using magnetic saturation is also proposed. The feasibility of the proposed sensorless method was verified by experimental results with the prototype SMIIR.**

I. INTRODUCTION

Information of rotor flux position is necessary to perform vector control of AC machine [1]. But position sensors like encoder, resolver, and etc., increase cost and volume of a machine and cause reliability issues of the sensor and its associated hardware. Therefore methods to find out the rotor flux position without a position sensor has been researched over 30 years and called as position sensorless methods [2]-[3]. These methods are generally classified in two groups depending on the principal on which the rotor flux position information is extracted. First group is based on the back electromotive force (EMF) [4]-[6], and the other group is based on the saliency of the rotor, mainly on magnetic saliency related to the mechanical structure of the machine itself [7]-[24].

The second group extracts the rotor flux position information from the relationship between the high-frequency stator voltage and stator current. With the saliency of rotor, the rotor flux position information is included in this relationship. Some of the second group use PWM current ripple [7]-[10], and others of this group use discontinuous signal [11]. The others use high-frequency signal [12]-[23]. These high-frequency signal injection sensorless methods have two injection algorithms: rotating voltage signal injection in the stationary reference frame [12]-[14], and pulsating voltage signal injection in the rotor reference frame [15]-[23]. And because these methods cannot distinguish the magnetic polarity, another mean to detect the magnetic polarity at initial state based on the magnetic saturation had been developed [24].

But these second group, relying on the magnetic saliency of the rotor, cannot applied to the machine which has no physical magnetic saliency. Although there has been a research based not on the saliency on the inductance due to different magnetic coupling but on the high-frequency resistance due to skin effect by the injected high frequency, it can be applicable to small size machine where the resistance is comparable to the impedance of the inductance [25].

Meanwhile, as the cost and availability of the rare earth materials are rapidly endangered, which are the indispensable in the manufacturing the permanent magnet, there have been many researches to develop new type of AC of machines to replace the permanent magnet synchronous machine (PMSM). One of these researches is the Synchronous Machine with an Inverter Integrated Rotor (SMIIR) [26]. The SMIIR is based on the conventional wound rotor synchronous machine (WRSM), but its stator and rotor windings are connected to a stator-side inverter and a rotor-side inverter, respectively. And the rotor-side inverter is integrated inside the rotor of SMIIR. The SMIIR has nearly same characteristics of the WRSM which has a large flux weakening region and a high efficiency in the region due to controllability of its field current. But SMIIR has no brushes and slip-rings, and no mechanical problems related to them: contact loss, wear, longer axial length, less reliability and less power density issue. The rotor-side inverter of the SMIIR has no power source and electrically isolated from the outside of rotor. Therefore, the electric power for the rotor-side inverter have to be transferred from the stator-side inverter to the rotor-side inverter. To transfer the power, the stator-side inverter injects high-

978-1-4673-4355-8/13/$31.00 ©2013 IEEE

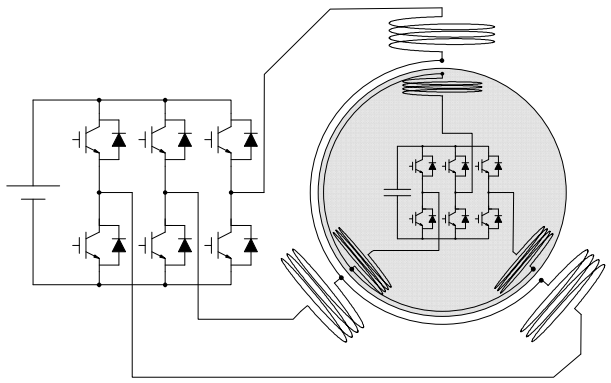

Figure 1. Structure of the SMIIR.

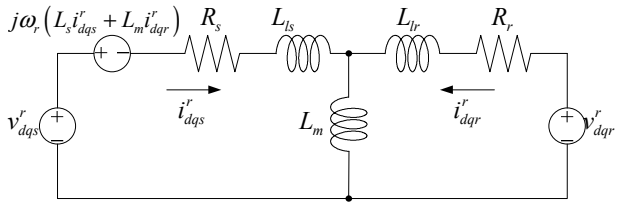

Figure 2. Equivalent circuit of the SMIIR in the d-q rotor reference frame.

frequency voltage in rotor reference frame and the rotor-side inverter controls high-frequency current properly to maintain its DC link voltage.

Because the SMIIR was newly introduced, there has been no research about position sensorless control of the SMIIR. In this paper, a signal injection sensorless method for the SMIIR is proposed. This method creates virtual resistance saliency using the rotor-side inverter. Based on this virtual saliency, a high-frequency signal injection sensorless method can be applied to the SMIIR, even though there is no sufficient physical magnetic saliency in SMIIR. This virtual saliency is independent of physical machine parameter, and axes of virtual saliency can be set arbitrarily. The proposed sensorless method works on the inherent high-frequency stator voltage, which is injected to transfer power to the rotor-side inverter in SMIIR. The voltage can not only transfer power to the rotor-side inverter but also cause current response which contains rotor position information. And an initial +d-axis detection algorithm without using magnetic saturation is also devised. The feasibility of the proposed method is verified by experimental test on the prototype SMIIR with associated control system.

II. Operation Principle of SMIIR

The SMIIR is based on an wound rotor synchronous motor, but an inverter is integrated inside the rotor, as shown in Fig. 1. The rotor-side inverter consists of DC link capacitor and switching devices and its own controller. And the rotor-side inverter rotates synchronously as the rotor rotates and is electrically isolated from the outside of the rotor. Therefore, there is no brush and slip-ring. This is the main difference between the SMIIR and the conventional wound rotor synchronous machine.

The equivalent circuit of the SMIIR in the d-q rotor reference frame is shown in Fig. 2. The voltage source v_{dqs} and v_{dqr} denote the output voltages of the stator-side and the rotor-side inverters respectively. i_{dqs} and i_{dqr} denote the current of the stator-side and the rotor-side inverters respectively. The superscript r denotes that corresponding variable is expressed in rotor reference frame, and ω_r denotes electrical angular frequency of the rotating speed of the rotor. The voltage equations of SMIIR can be derived as (1) and (2).

$$v^r_{dqs} = R_s i^r_{dqs} + \frac{d}{dt}\left(L_s i^r_{dqs} + L_m i^r_{dqr}\right) + j\omega_r\left(L_s i^r_{dqs} + L_m i^r_{dqr}\right), \quad (1)$$

$$v^r_{dqr} = R_r i^r_{dqr} + \frac{d}{dt}\left(L_r i^r_{dqr} + L_m i^r_{dqs}\right), \quad (2)$$

where $L_s = L_m + L_{ls}$, $L_r = L_m + L_{lr}$.

Although the SMIIR has a different rotor-side structure, basic operating principle of the SMIIR remains nearly same to the wound rotor synchronous machine. That is, the rotor-side inverter controls the rotor current, i^r_{dqr}, as DC in rotor reference frame to build a field flux. And torque of the machine can be controlled by regulating the stator current orthogonal to the field flux. In the constant torque region, the d-axis rotor current, i^r_{dr}, is set to the rated value and controlled as constant, and the q-axis stator current, i^r_{qs}, are controlled to build the required torque. And the q-axis rotor current, i^r_{qr}, and the d-axis stator current, i^r_{ds}, are regulated as null to minimize copper losses of the machine.

Because no power source is connected to the rotor-side inverter, the rotor-side inverter should be powered by means of electromagnetic coupling between the stator winding and rotor winding. For this purpose, the high-frequency voltage and current can be used to transfer the power from the stator-side inverter to the rotor-side inverter. The stator-side inverter generates the high-frequency stator voltage, v^r_{dqsh}, and the rotor-side inverter regulates the high-frequency rotor current, i^r_{dqrh}, according to the phase of the high-frequency stator voltage. To maximize efficiency of the power transfer, the phase difference between the high-frequency rotor current, i^r_{dqrh}, and the injected high-frequency stator voltage, v^r_{dqsh}, is controlled as 180 degrees. Moreover, the frequency of the power transfer should be high enough than cutoff frequency of the current controller to avoid interference between the torque control and the power transfer.

Each inverter has to perform different control scheme depending on the frequency range: fundamental frequency components for the machine drive and high-frequency components for the power transfer. The d-axis output voltages of the stator-side and the rotor-side inverters, can be written as (3) and (4), respectively.

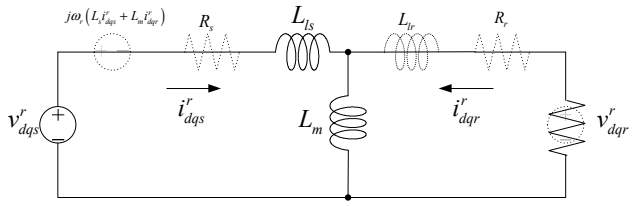

Figure 3. Equivalent circuit of SMIIR in the d-q rotor reference frame for the injected high-frequency.

$$v^r_{ds} = v^r_{dsl} + v^r_{dsh}\,, \tag{3}$$

$$v^r_{dr} = v^r_{drl} + v^r_{drh}\,, \tag{4}$$

where the subscripts *l* and *h* denote the low-frequency and the high-frequency components of the voltages, respectively. Under the assumption that the motor can be regarded as a linear system, the d-axis currents of the stator-side inverter and the rotor-side inverter are also divided into the same frequency components. The low-frequency and the high-frequency components of the currents can be expressed as (5) and (6), respectively.

$$i^r_{ds} = i^r_{dsl} + i^r_{dsh}\,. \tag{5}$$

$$i^r_{dr} = i^r_{drl} + i^r_{drh}\,. \tag{6}$$

Substituting (3)-(6) to (1) and (2), the voltage equations can be divided into low-frequency component and high-frequency component. The voltage equation for the high-frequency components can be presented in phasor variables as (7) for a steady state analysis.

$$\mathbf{V}^r_{dsh} = \left(jX_s + R_s\right)\mathbf{I}^r_{dsh} + jX_m\mathbf{I}^r_{drh}\,, \tag{7}$$

where the bold capital letters mean phasor variables and X means the reactance at the injected high-frequency, ω_h.

Because the high-frequency reactance X is much larger than the stator resistance, R_s, and the injected high-frequency, ω_h, is much larger than the electrical angular frequency, ω_r, (7) can be approximated as (8) and by the same way, the q-axis voltage equation can be approximated as (9).

$$\mathbf{V}^r_{dsh} \approx jX_s\mathbf{I}^r_{dsh} + jX_m\mathbf{I}^r_{drh}\,. \tag{8}$$

$$\mathbf{V}^r_{qsh} \approx jX_s\mathbf{I}^r_{qsh} + jX_m\mathbf{I}^r_{qrh}\,. \tag{9}$$

As mentioned before, to maximize the efficiency of the power transfer, the phase of the high-frequency rotor current is controlled out of phase to the injected high-frequency stator voltage as (10). Then, an equivalent circuit in this control mode can be depicted as Fig. 3.

$$\boldsymbol{I}^r_{dqrh} = -k\boldsymbol{V}^r_{dqsh}\,, \tag{10}$$

where k is a positive control constant. From (10), *k* can be seen as a negative virtual conductance.

III. Proposed Sensorless Method

A. Virtual Resistance Saliency

In the SMIIR, the high-frequency voltage is injected by the stator-side inverter, to transfer the power to the rotor-side inverter. Because the high-frequency voltage is already injected by the stator-side inverter, the high-frequency signal injection sensorless method can be applied without additional signals.

The conventional high-frequency signal injection sensorless methods are based on the physical magnetic saliency. The rotor position can be extracted from the relationship between the injected voltage, v^r_{dqsh}, and the response of the stator current, i^r_{dqsh} according to this saliency. Because the SMIIR has electro-magnetic symmetry similar to a WRSM or an induction machine (IM), the high-frequency signal injection sensorless method cannot be directly applied to the SMIIR.

Different from the other machines, the SMIIR has the rotor-side inverter which can create virtual saliency. That is, with proper control of the rotor-side inverter, response of the rotor current can be regulated similarly to a machine with the physical saliency in the rotor. For example, if the rotor-side inverter synthesize output voltage as (11), the rotor-side inverter responses as a virtual inductance.

$$v^r_{dqrh} = L_{dq}\frac{di^r_{dqrh}}{dt}\,, \tag{11}$$

By setting the virtual inductance L differently as (12) and (13), the rotor can reveal saliency on its inductance according to the rotor position.

$$v^r_{d_{inj}h} = L_{d_{inj}}\frac{di^r_{d_{inj}rh}}{dt}\,, \tag{12}$$

$$v^r_{q_{inj}h} = L_{q_{inj}}\frac{di^r_{q_{inj}rh}}{dt}\,, \tag{13}$$

where d_{inj} and q_{inj} denote axis where the maximum and minimum values of inductance exist, respectively. Because the virtual saliency is independent on the physical saliency, axes of saliency, d_{inj} - and q_{inj} -axis, can be arbitrarily placed for the sensorless control. If the virtual inductances are emulated according to (12) and (13), there should be extra voltages in the rotor-side inverter, and they may degrade the efficiency of the power transfer between the stator-side inverter and the rotor-side inverter. However, the rotor-side inverter of the SMIIR responses already as a negative resistance at the high frequency to receive the power from the stator. Therefore, the virtual resistance can be used to generate the saliency instead of the virtual inductance for the sensorless drive. The saliency of the virtual resistances can be set as (14) and (15).

$$\boldsymbol{I}^r_{d_{inj}rh} = -k_{d_{inj}}\boldsymbol{V}^r_{d_{inj}sh}\,, \tag{14}$$

$$\boldsymbol{I}^r_{q_{inj}rh} = -k_{q_{inj}}\boldsymbol{V}^r_{q_{inj}sh}\,, \tag{15}$$

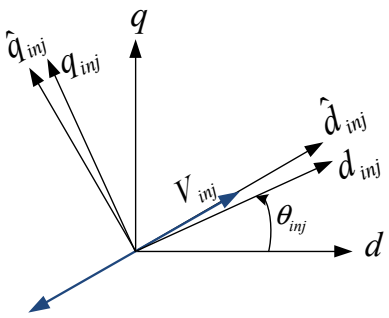

Figure 4. Diagram of high-frequency voltage injection scheme.

where $k_{d_{inj}}$ and $k_{q_{inj}}$ represent the virtual conductances and the values are difference from each other to generate artificial saliency of the rotor according to the rotor position. Thus the sensorless drive can be performed using the saliency of the virtual resistance regardless the physical saliency.

The saliency of the virtual resistances is not related to physical machine. Therefore it is not affected by operating conditions such as stator and rotor currents, rotating speed, load torque, and temperature as long as the amount of power transferred to the rotor-side inverter remains the same.

B. Sensorless method with saliency of the virtual resistance

The relationship between the d_{inj} -axis where the maximum or minimum virtual resistance exists and the d-axis where the field flux exists is shown in Fig. 4. The variable θ_{inj} represents the angle difference between the intended injection axis, d_{inj} , where the high frequency signal is intended to inject and the real rotor d-axis. And the symbol "^" denotes that the corresponding variable is an estimated value. For convenient explanation, d_{inj} - and q_{inj} -axes are named as saliency reference frame and $\hat{d}_{inj}$ - and $\hat{q}_{inj}$ -axes are referred as estimated saliency reference frame.

The high-frequency voltage for the power transfer can be injected along with the estimated saliency reference d-axis, $\hat{d}_{inj}$ -axis, as (16).

$$\begin{bmatrix} v^{\hat{r}}_{d_{inj}sh} \\ v^{\hat{r}}_{q_{inj}sh} \end{bmatrix} = V_{inj} \begin{bmatrix} \sin(\omega_h t) \\ 0 \end{bmatrix}. \tag{16}$$

Then, according to the relationship between the saliency reference frame and the estimated saliency reference frame, the injected high-frequency voltage can be expressed in the saliency reference frame as (17).

$$\begin{bmatrix} v^{r}_{d_{inj}sh} \\ v^{r}_{q_{inj}sh} \end{bmatrix} = \begin{bmatrix} \cos\tilde{\theta}_r & \sin\tilde{\theta}_r \\ -\sin\tilde{\theta}_r & \cos\tilde{\theta}_r \end{bmatrix} \begin{bmatrix} v^{\hat{r}}_{d_{inj}sh} \\ v^{\hat{r}}_{q_{inj}sh} \end{bmatrix} = V_{inj} \begin{bmatrix} \cos\tilde{\theta}_r \sin(\omega_h t) \\ -\sin\tilde{\theta}_r \sin(\omega_h t) \end{bmatrix}. \tag{17}$$

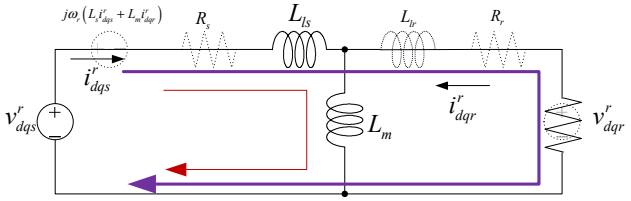

Figure 5. High-frequency current path.

where $\tilde{\theta}_r = \theta_r - \hat{\theta}_r$ denotes angle error between the actual rotor d-axis, d , and the estimated d-axis, $\hat{d}$. And, the angle error, $\tilde{\theta}_r$, also coincides with the angle difference between the angle, θ_{inj} , of the intended injection axis, d_{inj} , and the angle, $\hat{\theta}_{inj}$, of the actual injection axis, $\hat{d}_{inj}$, where actually the signal is injected**.**

Substituting (17) to (14) and (15), the high-frequency rotor current in saliency reference frame can be figured out as (18).

$$\begin{bmatrix} i^r_{d_{inj}rh} \\ i^r_{q_{inj}rh} \end{bmatrix} = -V_{inj} \begin{bmatrix} k_{d_{inj}} \cos\tilde{\theta}_r \sin(\omega_h t) \\ -k_{q_{inj}} \sin\tilde{\theta}_r \sin(\omega_h t) \end{bmatrix}. \tag{18}$$

Substituting (17) and (18) to (8) and (9), the high-frequency stator currents in saliency reference frame can be obtained as (19),

$$\begin{bmatrix} i^r_{d_{inj}sh} \\ i^r_{q_{inj}sh} \end{bmatrix} = -\frac{V_{inj}}{X_s} \begin{bmatrix} \sqrt{X_m{}^2 k_{d_{inj}}{}^2 + 1} \cos\tilde{\theta}_r \sin(\omega_h t + \psi_{d_{inj}}) \\ -\sqrt{X_m{}^2 k_{q_{inj}}{}^2 + 1} \sin\tilde{\theta}_r \sin(\omega_h t + \psi_{q_{inj}}) \end{bmatrix}, \tag{19}$$

where $\psi_{d_{inj}} = \tan^{-1}(\frac{1}{X_m k_{d_{inj}}}) + \pi$ and $\psi_{q_{inj}} = \tan^{-1}(\frac{1}{X_m k_{q_{inj}}}) + \pi$ denote the phase differences between the high-frequency stator voltages and the high-frequency stator currents in saliency reference d- and q-axis, respectively.

In practice, $X_m k_{d_{inj}}$ and $X_m k_{q_{inj}}$ are much larger than unity because the reactance at the injected high-frequency is much larger than the corresponding resistances which are the inverse of the conductances, $k_{d_{inj}}$ and $k_{q_{inj}}$. Thus, the current path at the high-frequency is not through the magnetizing inductance but the through the virtual resistance as shown in Fig. 5. And, the phase differences, $\psi_{d_{inj}}$ and $\psi_{q_{inj}}$, can be approximated to π . In conclusion, the high-frequency stator currents in the estimated saliency reference frame can be derived as (20).

$$\begin{bmatrix} i^{\hat{r}}_{d_{inj}sh} \\ i^{\hat{r}}_{q_{inj}sh} \end{bmatrix} = \begin{bmatrix} \cos\tilde{\theta}_r & -\sin\tilde{\theta}_r \\ \sin\tilde{\theta}_r & \cos\tilde{\theta}_r \end{bmatrix} \begin{bmatrix} i^{r}_{d_{inj}sh} \\ i^{r}_{q_{inj}sh} \end{bmatrix}$$

$$\approx \frac{X_m V_{inj}}{X_s} \begin{bmatrix} k_{d_{inj}} \cos^2\tilde{\theta}_r \sin(\omega_h t) + k_{q_{inj}} \sin^2\tilde{\theta}_r \sin(\omega_h t) \\ \frac{\sin 2\tilde{\theta}_r}{2}(k_{d_{inj}} - k_{q_{inj}})\sin(\omega_h t) \end{bmatrix} \cdot \quad (20)$$

Because the magnitude of the stator current in the estimated saliency reference q-axis, $i^{\hat{r}}_{q_{inj}sh}$, includes the angle error, $\tilde{\theta}_r$, the angle error can be extracted by a simple demodulation process as (21).

$$\varepsilon_f = LPF(i^{\hat{r}}_{q_{inj}sh} \sin\omega_h t) \approx \frac{X_m V_{inj}}{4X_s} \sin 2\tilde{\theta}_r (k_{d_{inj}} - k_{q_{inj}}), \quad (21)$$

where LPF represents low-pass filtering process to eliminate the $2\omega_h$ frequency component from the signal inside of the parenthesis. Moreover, if the estimated angle error is small enough, (21) can be further approximated as (22).

$$\varepsilon_f \approx \frac{X_m V_{inj}}{2X_s}(k_{d_{inj}} - k_{q_{inj}})\tilde{\theta}_r . \quad (22)$$

Therefore the position error can be extracted from the high-frequency component of the stator current. And using an appropriate state observer, the rotor position can be identified from the position error information [21].

C. *Initial +d-axis detection*

As seen from (21), because the rotor position error information, ε_f, is a function of two times of angle error, $\tilde{\theta}_r$, +d-axis and –d-axis cannot be distinguishable and additional initial +d-axis detection method should be devised. The conventional high-frequency signal injection sensorless method uses asymmetry of the d-axis inductance due to the magnetic saturation. However, because the proposed method is based on the saliency of the virtual resistance, the conventional methods cannot be applicable directly.

Contrast to the conventional machine, by exploiting the controllability of the rotor current, asymmetric current response can be forced by the rotor-side inverter of SMIIR. Using the asymmetric current response, the polarity of d-axis can be found. Although the asymmetric current response can be implemented in both d_{inj} - and q_{inj} -axes, the q_{inj} -axis is only used for the polarity detection because the d_{inj} -axis stator current has already high-frequency signal due to power transfer and sensorless control. Therefore during the time of initial angle detection, the q_{inj} -axis rotor current is regulated by the rotor-side inverter to send a signal to let the stator-side inverter identify whether the estimated rotor position is +d-axis or not.

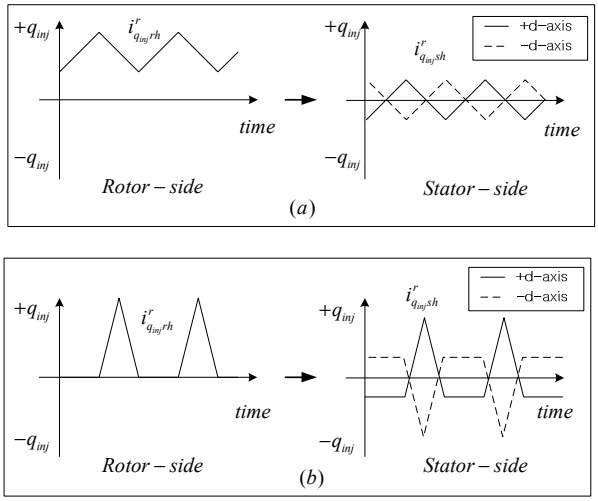

Figure 6. Current response in the rotor and stator according to the polarity of d-axis.
(a) Case of symmetric AC current with DC. (b) Case of asymmetric AC current.

Table 1. Machine Parameters of WRIM modified to SMIIR

Nominal Parameters	Power	9 [kW]
	Poles	6
	Speed	1165 [r/min]
	Voltage	220 [V_{rms}]
	Stator Current	44 [A_{rms}]
	Rotor Current	29 [A_{rms}]
DC parameter	Rs / Rr	0.112 / 0.09 [Ω]
High-frequency parameter (f_{inj} = 500Hz)	Lls, Llr	0.97 [mH]
	Lm	14.3 [mH]
Control parameter	V_{inj}	25 [V_{peak}]
	$k_{d_{inj}}$ / $k_{q_{inj}}$	0.1 / 0.15 [S]

Because rotor current signal is sent by magnetic mutual coupling between stator and rotor winding, only AC components are transferred from the rotor to the stator. That is, when deciding the shape of the rotor current signal, symmetric AC signal biased with DC is not useful because high-frequency stator current according to +d-axis or -d-axis is not distinguishable as shown in Fig. 6(a). As a proper signal, a pulse signal can be used to exaggerate asymmetry of the signal. If the average of the signal is small enough, the peak signal can be transferred to the stator without severe distortion. If the rotor-side inverter makes $+q_{inj}$ -axis peak current and the stator-side inverter senses $+q_{inj}$ -axis peak current, then the estimated rotor position is in the +d-axis. Otherwise, if the stator-side inverter senses $-q_{inj}$ -axis peak current, then the estimated rotor position is in the -d-axis as shown in Fig. 6(b).

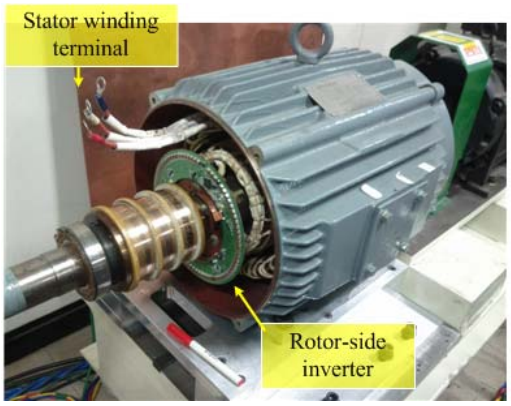

Figure 7. Experimental test machien : SMIIR

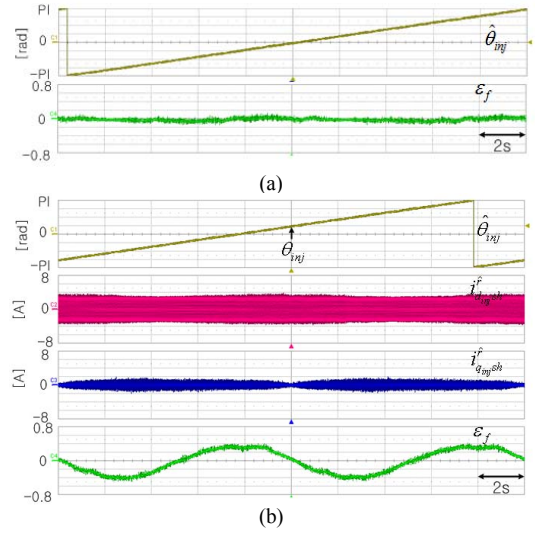

Figure 8. Engle error charateristics as injetion angle changes.
(a) without virtual salinecy; original saliency of the SMIIR.
(b) with proposed virtual resistance saliency.

IV. EXPERIMENTAL RESULT

To figure out the feasibility of the proposed sensorless method for the SMIIR, experiments has been carried out. The parameters of the test machine are shown in Table 1. Test machine is modified from an off-the-shelf wound rotor induction machine (WRIM) and the diameter of the rotor-side inverter is about 20cm as shown in Fig.7.

Fig. 8 shows experimental results verifying (21). The angle of injected voltage, $\hat{\theta}_{inj}$, slowly changes from –π to π to confirm the electrical saliency. As shown in Fig. 8(a), the SMIIR reveals no saliency for a sensorless control. While, as shown in Fig. 8(b) the waveforms of $\hat{\theta}_{inj}$, $i^{\hat{r}}_{d_{inj}sh}$, $i^{\hat{r}}_{q_{inj}sh}$,and ε_f clearly reveal the salient responses. In this experiment the intended injection angle, θ_{inj} , is set as $\pi/4$. And, as mentioned in III B, $\hat{\theta}_r = \hat{\theta}_{inj} - \pi/4$. Hence, (21) can be

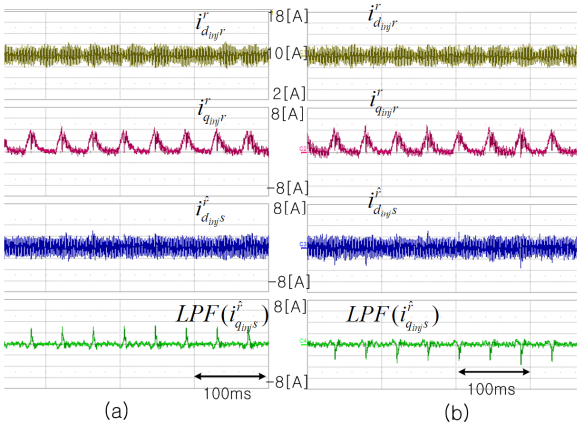

Figure 9. Experiment resulf of initial +d-axis detection at standstill.
(a) the estimated d-axis is aligned to the +d-axis. (b) the estimated d-axis is aligned to the -d-axis.

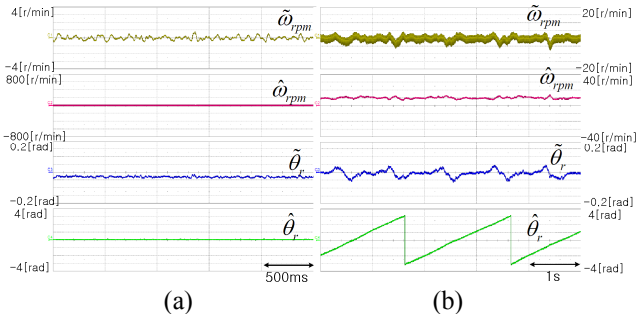

Figure 10. Experimentral result of speed control at steady state with no load.
(a) standstill. (b) 10r/min.

confirmed from Fig. 8(b). From the fact that when $\hat{\theta}_{inj}$ is ahead of θ_{inj} , ε_f is negative, and when $\hat{\theta}_{inj}$ is behind of θ_{inj} , ε_f is positive, rotor position can be tracked with a simple error correction controller whose input is ε_f .

Fig. 9 shows experimental result of initial +d-axis detection. The proposed sensorless method settles down at either +d-axis or –d-axis depending on the initial condition. In this experiment the intended injection angle, θ_{inj} , is set as zero. The rotor-side inverter controls the DC component of i^r_{dr} to build up the field flux and the high-frequency component of $i^r_{d_{inj}r}$ to the power transfer. Meanwhile, during initial angle detection period, $i^r_{q_{inj}r}$ is controlled as a pulse to distinguish the polarity of the d-axis. After initial angle detection, $i^r_{q_{inj}r}$ is regulated to zero to reduce the copper loss. Because $i^{\hat{r}}_{q_{inj}s}$ has undesired signal noise, $LPF(i^{\hat{r}}_{q_{inj}s})$ is used to distinguish +d-axis and –d-axis. Fig. 9(a) and (b) represent the case when the estimated d-axis is aligned to +d-axis and –d-axis, respectively. As comparing the sign of the peaks,

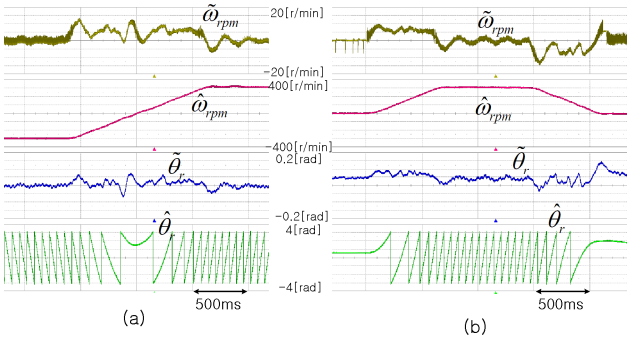

Figure 11. Experimental result of dynamic speed control with no load. (a) -300 -> 300 [r/min] . (b) 0 -> 300 ->0 [r/min].

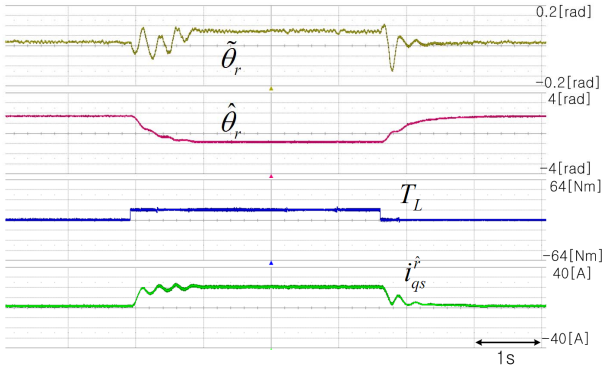

Figure 12. Experimental result of step load torque(1/3 of rated torque) response at standstill speed control.

+d-axis can be found with the devised initial +d-axis detection method.

Fig. 10 depicts experimental results of speed control with the proposed sensorless method at steady state under no load condition. $\tilde{\omega}_{rpm}$, $\hat{\omega}_{rpm}$, $\tilde{\theta}_r$, and $\hat{\theta}_r$ represent estimated speed error, estimated speed, estimated electrical angle error, and estimated electrical angle, respectively. At standstill, the speed error was less than 1r/min while the electric angle error was less than 0.05rad as shown in Fig. 10(a). At 10r/min, the speed error was less than 5r/min while the angle error was less than 0.05rad as shown in Fig. 10(b).

Fig. 11 shows experimental results of dynamic speed control with no load. While the motor speed varies from -300r/min to 300r/min, the speed error was less than 13r/min and the electric angle error was less than 0.1rad as shown in Fig. 11(a). While the motor speed changes from 0r/min to 300r/min and then back to 0r/min, the speed error was less than 15r/min and angle error was less than 0.15rad as shown in Fig. 11(b).

Fig. 12 shows experimental result of step load torque response at standstill speed control. The load torque is one third of the rated torque and therefore q-axis current is also one third of rated stator current. During the step load torque response, angle error was less than 0.15rad.

V. CONCLUSION

In this paper, a sensorless method for SMIIR has been proposed. This method creates virtual resistance saliency using the rotor-side inverter for the SMIIR, of which magnetic saliency is not sufficient for high-frequency signal injection method. Because this artificially generated virtual saliency is independent of physical saliency, axes of saliency can be arbitrarily placed.

Using the proposed virtual resistance saliency, rotor position information can be extracted in relationship between the high-frequency stator voltage and current. Because the SMIIR already injects high-frequency voltage to transfer electrical power to the rotor-side inverter, there is no need to inject additional voltage for high-frequency sensorless method. Also, an initial +d-axis detection algorithm using the artificial asymmetry of the current response by the rotor-side inverter has been devised.

The proposed method has been verified by an experimental test with the prototype SMIIR. The electrical angle error characteristics, initial +d-axis detection algorithm, and the speed control performance under various operating conditions have been verified. The proposed sensorless control method for SMIIR might enhance the applicability of SMIIR to industrial field such as traction machine for road vehicles and generators for conventional and renewable energy system.

REFERENCES

[1] D. W. Novotny, and T. A. Lipo, “Vector control and dynamics of AC drives,” Clarendon Press, Oxford, 1996.

[2] J. Holtz, “Sensorless control of induction machines-with or without signal injection?,” IEEE Trans. Ind. Electron., vol. 53, no. 1, pp. 7-30, Feb. 2006.

[3] P. P. Acarnley, and J. F. Watson, “Review of position-sensorless operation of brushless permanent-magnet machines,” IEEE Trans. Ind. Electron., vol. 53, no. 2, pp. 352-362, Apr. 2006.

[4] S. Ogasawara and H. Akagi, “An approach to position sensorless drive for brushless dc motor,” IEEE Trans. Ind. Appl., vol. 27, no. 5, pp. 928–933, Sep./Oct. 1991.

[5] K. D. Hurst, T. G. Habetler, G. Griva, and F. Profumo, “Zero-speedtacholess IM torque control: Simply a matter of stator voltage integration,”IEEE Trans. Ind. Appl., vol. 34, no. 4, pp. 790–795, Jul./Aug. 1998.

[6] R. B. Sepe and J. H. Lang, “Real-time observer-based (adaptive) control of a permanent-magnet synchronous motor without mechanical sensors,” IEEE Trans. Ind. Appl., vol. 28, no. 6, pp. 1345–1352, Nov./Dec. 1992.

[7] A. B. Kulkarni and M. Ehsani, “A novel position sensor elimination technique for interior permanent-magnet synchronous drive,” IEEE Trans. Ind. Appl., vol. 28, no. 1, pp. 144–150, Jan./Feb. 1992.

[8] V. Petrovic, A. M. Stankovic, and V. Blasko, “Position estimation in salient PM synchronous motors based on PWM excitation transients,” IEEE Trans. Ind. Appl., vol. 39, no. 3, pp. 835-843, May/Jun. 2003.

[9] M. Mamo, K. Ide, M. Sawamura, and J. Oyama, “Novel rotor position extraction based on carrier frequency component method (CFCM) using two reference frames for IPM drives,” IEEE Trans. Ind. Electron., vol. 52, no. 5, pp. 508-514, Apr. 2005.

[10] S. Ogasawara, and H. Akagi, “Implementationand position control performance of a position-sensorless IPM motor drive system based on magnetic saliency,” IEEE Trans. Ind. Appl., vol. 34, pp. 806-812, Jul./Aug. 1998.

[11] M. Schroedl, "Sensorless control of AC machine at low speed and standstill based on the 'INFORM' method," in Conf. Rec. IEEE-IAS Annu. Meeting, 1996, pp. 270-277.

[12] P. L. Jansen, and R. D. Lorenz, "Transducerless position and velocity estimation in induction and salient AC machines," IEEE Trans. Ind. Appl., vol. 31, no. 2, pp. 240-247, Mar./Apr. 1995.

[13] S. Kim, Y.-C. Kwon, S.-K. Sul, J. Park, and S.-M. Kim, "Position sensorless operation of IPMSM with near PWM switching frequency signal injection," in Proc. of ICPE2011-ECCE Asia, 2011.

[14] Y. Jeong, R. D. Lorenz, T. M. Jahns, and S. K. Sul, "Initial rotor position estimation of an interior permanent-magnet synchronous machine using carrier-frequency injection methods," IEEE Trans. Ind. Appl., vol. 41, no. 1, pp. 38–45, Jan./Feb. 2005.

[15] J. I. Ha and S. K. Sul, "Sensorless field-orientation control of an induction machine by high-frequency signal injection," IEEE Trans. Ind. Appl., vol. 35, no. 1, pp. 45–51, Jan./Feb. 1999.

[16] J. I. Ha, K. Ide, T. Sawa, and S. K. Sul, "Sensorless position control and initial position estimation of an interior permanent magnet motor," in Conf. Rec. IEEE IAS Annu. Meeting, Sep. 2001, vol. 4, pp. 2607–2613.

[17] J. H. Jang, S. K. Sul, J. I. Ha, K. Ide, and M. Sawamura, "Sensorless drive of surface-mounted permanent-magnet motor by high-frequency signal injection based on magnetic saliency," IEEE Trans. Ind. Appl., vol. 39, no. 4, pp. 1031–1039, Jul./Aug. 2003.

[18] K. Ide, J. K. Ha, and M. Sawamura, "A hybrid speed estimation of flux observer for induction motor drives," IEEE Trans. Ind. Electron., vol. 53, no. 1, pp. 130–137, Feb. 2006.

[19] M. J. Corley, and R. D. Lorenz, "Rotor position and velocity estimation for a salient-pole permanent magnet synchronous machine at standstill and high speeds," IEEE Trans. Ind. Appl., vol. 34, no. 4, pp. 784-789, Jul./Aug. 1998.

[20] R. Leidhold, and P. Mutschler, "Improved method for higher dynamics in sensorless position detection," in Proc. IEEE IECON2008, 2008, pp. 1240-1245.

[21] Y.-D. Yoon, S.-K. Sul, S. Morimoto, and K. Ide, "High bandwidth sensorless algorithm for AC machines based on square-wave-type voltage injection," IEEE Trans. Ind. Appl., vol. 47, no. 3, pp. 1361-1370, May/Jun. 2011.

[22] R. Masaki, S. Kaneko, M. Hombu, T. Sawada, and S. Yoshihara, "Development of a position sensorless control system on an electric vehicle driven by a permanent magnet synchronous motor," in Proc. IEEE PCC Osaka 2002, vol. 2, 2002, pp. 571-576.

[23] S. Kim, J. I. Ha, S.K. Sul, "PWM Switching Frquency Signal Injection Sensorless Method in IPMSM," IEEE Trans. Ind. Appl., Vol. 48, No. 5, Sep./Oct. 2012

[24] J. I. Ha, K. Ide, T. Sawa, and S. K. Sul, "Sensorless rotor position estimation of an interior permanent-magnet motor from initial states," IEEE Trans. Ind Appl., Vol. 39, No. 3, pp. 761-767, May-June 2003.

[25] D. D. Reigosa, P. Garcia, F. Birz, D. Raca, R. D. Lorenz, "Modeling and Adaptive Decoupling of High-frequency Resistacne and Temperature Effects in Carrier-Based Sensorless Control of PM Synchronous Machines," IEEE Trns. Ind. Appl., Vol. 46, No. 1, Jan./Feb. 2010

[26] E. Jung, S. Kim, J. I. Ha, S. K. Sul, "Control of a Synchronous Motor with an Inverter Integrated Rotor," scheduled to be published in IEEE Trans. Industry Applications, Oct. 2012.